Available online at www.sciencedirect.com
SCIENCE DIRECT
Journal of Molecular Structure 795 (2006) 256–262
Journal of MOLECULAR STRUCTURE
www.elsevier.com/locate/molstruc

Gas-phase detection of HSOD and empirical equilibrium structure of oxadisulfane

Oliver Baum [a], Simone Esser [b], Niels Gierse [a], Sandra Brünken [a,1], Frank Lewen [a], Josef Hahn [b], Jürgen Gauss [c], Stephan Schlemmer [a], Thomas F. Giesen [a,*]

[a] I. Physikalisches Institut, Universität zu Köln, Zülpicher Strasse 77, 50937 Köln, Germany
[b] Institut für Anorganische Chemie, Universität zu Köln, Greinstraße 6, 50939 Köln, Germany
[c] Institut für Physikalische Chemie, Universität Mainz, 55099 Mainz, Germany

Received 8 February 2006; received in revised form 16 February 2006; accepted 17 February 2006
Available online 17 April 2006

This paper is dedicated to Prof. Gisbert Winnewisser on the occasion of his 70th birthday.

Abstract

We present the first gas phase spectra of singly deuterated oxadisulfane, HSOD, in its vibrational ground state. More than 100 transitions have been recorded with highest frequency accuracy using the Cologne Terahertz Spectrometer. The molecular parameters derived from a least squares fit analysis proof HSOD to be an almost accidental symmetric prolate top molecule with an asymmetry parameter $\kappa = -0.9985$. Spectra of *c*-type and weaker *b*-type transitions have been recorded in the range from 716 to 772 GHz. The ratio of the dipole moments $\mu_c/\mu_b = 2.4(3)$ has been derived from measured line intensities. The *c*-type transitions are split by the tunneling motion of a hindered internal rotation, whereas *b*-type transitions show no splitting within the Doppler limited line profiles. We derived the equilibrium molecular structure of oxadisulfane, HSOH, from experimental values of the rotational constants A_0, B_0, and C_0 of HSOH, $H^{34}SOH$, DSOD, and HSOD. The equilibrium rotational constants A_e, B_e, and C_e were derived by taking vibration–rotation interaction constants α_r obtained from high-level *ab initio* calculations into account.

Keywords: HSOD; oxadisulfane; HSOH; Molecular structure; Terahertz spectroscopy

1. Introduction

Hydrogen peroxide (HOOH), disulfane (HSSH), and oxadisulfane (HSOH) belong to a family of molecules which possess a simple skew-chain geometry. The two bond angles and the dihedral angle are all relatively close to 90°. While HOOH and HSSH have a C_2 symmetry axis oriented perpendicular to the bond of the two heavy atoms bisecting the dihedral angle, HSOH has no symmetry at all. The principal axis corresponding to the smallest moment of inertia, the *a*-axis, is in all three cases almost coincident with the bond between the two heavy atoms. Despite their asymmetric structure, these molecules are nearly accidental prolate symmetric tops with rotational constants $B \approx C$ corresponding to almost identical momenta of inertia $I_b \approx I_c$. These simple skew-chain molecules have two geometrical forms, which are mirror images of each other. Rotating one of the two hydrogen atoms by two times the dihedral angle τ about the *a*-axis transfers the molecules into their enantiomeric forms. The motion is hindered by a torsional potential with maxima at the molecule's *cis*-configuration (dihedral angle $\tau = 0°$), and at the *trans*-configuration where the two hydrogen bonds are pointing in opposite directions ($\tau = 180°$). The barrier heights for the *trans*-configuration have been found experimentally to be 387.07 cm^{-1} for HOOH [1] and 2037 cm^{-1} for HSSH [2], whereas the *trans* potential barrier of HSOH has been derived from high level *ab initio* calculations at the CCSD(T)/cc-pCVQZ level to be 1579 cm^{-1} [3]. In all cases, the *cis* tunnel barrier is higher than the *trans* barrier and of the order 2000–3000 cm^{-1}. The tunnel effect causes a splitting of each rotational energy level; this splitting depends on the potential barrier height and, to a lesser extent, on the rotational quantum numbers. The splitting in

* Corresponding author. Tel.: +49 221 470 4529; fax: +49 221 470 5162.
E-mail address: giesen@ph1.uni-koeln.de (T.F. Giesen).
[1] Present address: Harvard-Smithsonian Center for Astrophysics, 60 Garden Street, Cambridge, MA 02138, USA.

0022-2860/$ - see front matter © 2006 Elsevier B.V. All rights reserved.
doi:10.1016/j.molstruc.2006.02.037

the vibrational ground state is large for HOOH, intermediate for HSOH and small for HSSH.

A rotationally resolved spectrum of HSSH has been published as early as 1968 by Winnewisser *et al*. [4], and the tunnel splitting was found to be less than 100 kHz. In contrast, the splitting for HOOH is much larger and about 680 GHz (see [5]). Experimental data on gas phase HSOH became available only recently [3], and were for long time hampered by the difficulties of its synthesis. Smardzewski and Lin recorded infrared spectra of products from photolysis of ozone (O_3) and hydrogen sulfide (H_2S) trapped in an argon matrix and they assigned some of the spectral features to vibrational modes of HSOH [6]. Later on, Iraqi and Schwarz detected HSOH by mass spectroscopy in a chemical ionization source from an H_2S/N_2O gas mixture [7]. None of these syntheses were suited for gas phase detection of HSOD by means of absorption spectroscopy. The breakthrough came in 2003 when Behnke and Hahn [8] found a novel method of producing oxadisulfane in large quantities from flash vacuum pyrolysis of di-*tert*-butyl sulfoxide. Assisted by high-level quantum chemical calculations, Winnewisser *et al*. [3] recorded the first rotationally resolved gas phase spectra of HSOH and determined the tunnel splitting in the lowest rotational levels to be 64.5 MHz. In the same year, the authors also succeeded in recording the first gas phase spectra of the doubly deuterated species, DSOD [9]. The tunnel splitting obtained from measurements of ${}^rQ_0$ and ${}^rQ_2$ band transitions was found to be much smaller than for HSOH and less than 0.5 MHz, according to a lower zero point energy. These values are in good agreement with *ab initio* calculations published by Quack and Willeke [10], predicting a 70 MHz tunnel splitting for HSOH and a 0.34 MHz splitting in the case of DSOD. The experimental studies on DSOD were extended to higher frequencies by Brünken *et al*. [11] who measured the transitions of the ${}^rQ_3$-branch at 653 GHz.

In this paper, we present first spectroscopic data on singly deuterated oxadisulfane, HSOD, with the clear aim to derive precise molecular parameters. Furthermore, highly precise data from our previous measurements on HSOH, $H^{34}SOH$, and DSOD together with the new HSOD data are used to derive for the first time a semi-experimental, i.e. a so-called empirical structure of oxadisulfane. The S–O bond in molecules such as HSO, SO, or SO_2 is known to exhibit a multibond character with a bond length of approximately 1.45 Å, whereas classical S–O single bonds have lengths around 1.66 Å. Oxadisulfane is the simplest molecule which possesses a classical S–O single bond and is thus a testbed for high level *ab initio* calculations of S–O single bond molecules and of geometrical structure calculations in general (see e.g. [3,12–17]).

2. Synthesis of HSOD and experimental setup

Flash vacuum pyrolysis of di-*tert*-butyl sulfoxide is an efficient way of synthesizing HSOH for gas phase spectroscopy [3], although this method cannot be easily used to produce deuterated species of oxadisulfane. In our recent studies on perdeutero oxadisulfane, DSOD, we used a gas mixture of D_2S and D_2O introduced into a radio-frequency plasma [9,11] at typically 25 W discharge power. A constant gas flow at 1–5 Pa and a D_2O/D_2S ratio of 1:1 yielded best results for DSOD. We found that smaller amounts of D_2S are sufficient when a thin layer of sulfur starts to build up on the cell walls, and DSOD is formed even without any D_2S from D_2O when elementary sulfur powder is introduced into the rf-plasma region.

In the present work on HSOD, we used a constant flow of HDO from a stochiometric mixture of H_2O and D_2O which leads to a ratio $H_2O{:}HDO{:}D_2O = 1{:}2{:}1$. A small vessel containing elementary sulfur powder was inserted into the tube near the discharge region and HSOD was measured *in situ* through the rf-discharge plasma. During the experiments, we found the amount of HSOD tremendously increased at zero gas flow. For most of the measurements, the cell was thus filled to constant water pressures of 2–3 Pa and highest yields of HSOD were achieved at 25 W discharge power. The absorption signals disappeared immediately after switching off the rf-plasma and appeared as soon as the discharge was switched on, which indicates the residence time of HSOD to be fairly short under these conditions and less than some hundred milliseconds. Recently, Beckers *et al*. discussed various thermal decomposition routes of oxadisulfane (HSOH) and found H_2O and elementary sulfur to be the by far favored products of the bidirectional reaction $HSOH \rightleftharpoons H_2O + S$ [18]. This also seems to hold for HSOD produced in an rf-plasma and leads to a constant concentration of HSOD over hours, provided that stable plasma conditions are achieved.

Besides HSOD many other species are formed in the rf-plasma, among them sulfur containing molecules, such as H_2S, S_2O, SO_2, SO but also HSOH and DSOD due to the presence of H_2O and D_2O. To assign spectral lines of HSOD, we recorded spectra with pure H_2O and D_2O, respectively, to distinguish solely hydrogen and deuterium containing molecules from mixed products. Transitions which belong to HSOD disappeared completely under these conditions.

All spectra were recorded using the Cologne Terahertz Spectrometer, which has been described in detail in [19]. Briefly, the radiation of broadband tunable backward wave oscillators (BWOs) is used to record absorption spectra in the frequency range between 120 and 1100 GHz. The BWO is phase-locked to a Rubidium reference, resulting in a frequency stability of 10^{-11}. In the normal operation mode, the resolution is limited by the Doppler width of the lines, and an overall frequency accuracy of 10–500 kHz is achieved depending on the line-strength and on baseline effects. Spectra are recorded in 2f-mode and the radiation is detected with a phase-sensitive InSb hot electron bolometer cooled to liquid Helium temperature.

3. Theoretical predictions of rotational constants

Ab initio calculations predict oxadisulfane to be close to the case of an accidental prolate symmetric top molecule. The asymmetry of a molecule is quantified by Ray's asymmetry parameter $\kappa = (2B - A - C)/(A - C)$, where *A, B*, and *C* denote the rotational constants. The parameter κ equals -1 for a prolate symmetric top and $+1$ for an oblate symmetric

molecule. The asymmetry of HSOD is predicted based on quantum chemical calculations (see below) to be −0.9985, which is even closer to the limiting symmetric top case than HSOH ($\kappa_{exp} = -0.9953$).

The calculated rotational constants A_0, B_0, and C_0 needed for the theoretical prediction of the rotational spectrum of HSOD have been obtained from an approach described in our previous work, where it has been applied to HSOH and DSOD [3,9]. The corresponding equilibrium values (A_e, B_e, C_e) have been computed from highly accurate equilibrium geometries obtained using the coupled-cluster singles and doubles approach augmented by a perturbative treatment of triple excitations (CCSD(T)) [20] together with Dunning's core-polarized cc-pCVQZ basis set [21]. The corresponding vibrational corrections $\Delta B = B_0 - B_e$ have been calculated via the corresponding vibration–rotation interaction constants α_r [22] using second-order perturbation theory starting from the harmonic-oscillator rigid-rotor approximation. The needed quadratic and cubic force fields have been computed at the CCSD(T) level using the cc-pVTZ basis [23] employing analytic second-derivative techniques [24]. In addition, centrifugal distortion constants have been computed at the CCSD(T)/cc-pVTZ level of theory. Finally, the computed spectroscopic constants have been scaled with the experimental to theoretical ratios taken from HSOH and DSOD in order to improve the predictions.

The dipole moment μ is also obtained from these calculations and the strongest component, $\mu_c = 1.49$ D, is pointing along the *c*-axis. The μ_b component is weaker by a factor of 2 ($\mu_b = 0.79$ D), and the μ_a component is rather weak ($\mu_a = 0.01$ D). All values are similar to the values for HSOH (see [3]). We thus expect a clear-cut perpendicular spectrum with strong *c*-type transitions, weaker *b*-types and almost non-detectable *a*-type transitions.

4. Results and analysis

The ^rQ ($\Delta K_a = 1$, $\Delta J = 0$) branches of an asymmetric rotor exhibit characteristic patterns which allow for the unambiguous identification of new molecular species. Similar to the case of a symmetric top molecule perpendicular spectra of an almost accidental symmetric rotor have prominent *Q*-branches at frequencies of approximately $(A-(B+C)/2)(2K_a+1)$, where K_a has the values 0,1,2,… The location of the bandheads of the lowest branches of HSOD, $^rQ_{0,1,2}$ were derived from *ab initio* calculations to be at around 146, 438 and 729 GHz, respectively. In the course of this paper, we searched the spectral range from 716 to 772 GHz for $^rQ_2$ transitions of HSOD employing the Cologne Terahertz Spectrometer.

In total, 118 *Q*-branch rotational transitions of HSOD were measured. 94 lines have been assigned to *c*-type and 12 to *b*-type transitions. Line frequencies could be derived to accuracies between 100 and 300 kHz. The *c*-type transitions are stronger than the *b*-types according to the two times stronger dipole moment component in the *c*-axis direction. In addition to $^rQ_2$ lines 12 $R_{0,1}$-branch transitions were recorded which allowed to determine the rotational constants *A*, *B*, and *C* separately.

Each transition occurs as a doublet. The splitting is caused by the molecules internal tunneling motion through a potential barrier, which separates the left-handed from the right-handed conformer. The energy separation δ_{K_a} of corresponding levels depends on the K_a quantum number and is for HSOH in the order of 20–70 MHz for $0 \leq K_a \leq 4$ [25]. The tunnel splitting is much smaller for DSOD and could not be resolved in our recently published Doppler limited measurements [11]. HSOD transitions are expected to show a tunnel splitting which is larger than that of DSOD, but smaller compared to the HSOH splitting. A calculated value $\delta = 3.45$ MHz for the splitting in HSOD, which does not account for the K_a dependence, has been published by Quack and Willeke [10]. As a result, we searched for line doublets separated by a few Megahertz and found a series of paired lines with ~4.5 MHz separation which we assigned to *c*-type transitions of the $^rQ_2$ branch. As in the case of HSOH, we found the effect of tunnel splitting more prominent for *c*-type transitions compared to the *b*-types (see [3,25]). A series of weaker lines has been assigned to *b*-type transitions of the HSOD $^rQ_2$ branch for which the effect of tunnel splitting is not resolved within Doppler limited line profiles. Fig. 1 shows part of the recorded spectrum with the two tunnel splitting components of the $J = 20$ *c*-type and the not resolved *b*-type transition. The *b*-type transition is weaker than the *c*-type transition but gains in strength due to the overlapping tunnel components. A stick diagram indicates the calculated center positions and line strengths of the doublets. $^rQ_2$-branch transitions up to $J = 38$ have been measured and are depicted in the Fortrat diagram of Fig. 2. Full circles represent measured transitions while empty circles designate calculated line positions from a least-squares fit analysis of all data. The asymmetry splitting into two sub-branches is clearly visible and increases rapidly with *J* rotational quantum numbers. A smaller splitting separates *c*- and *b*-type transitions. The weaker *b*-types were partly overlapped by the *c*-type doublets and thus only few *b*-type transitions have been clearly identified in the spectral range. The effect of tunnel splitting is too small to be resolved in the Fortrat diagram.

Fig. 3 shows measured *c*-type transitions near the band center of the $^rQ_2$ branch. *b*-Type transitions are too weak to be seen in the spectra. In some cases, lines seen in the recorded spectra were overlapped by stronger transitions of other molecules and are not depicted in Fig. 3. A calculated spectrum is shown in the lower trace and has been derived from a least-squares fit analysis. The numbers below the calculated spectrum give *J* rotational quantum numbers of the *c*-type transitions. Each line is split by internal rotation into two equally spaced components separated by ~4.5 MHz. The upper row *J*-quantum numbers belong to the asymmetry component $J_{3,J-2} \leftarrow J_{2,J-2}$ while the two lower rows show transitions belonging to the asymmetry component $J_{3,J-3} \leftarrow J_{2,J-1}$. As can be seen from the Fortrat diagram in Fig. 2, the asymmetry component with $J_{3,J-3} \leftarrow J_{2,J-1}$ turns from higher to lower frequencies for *J* up to 23 and then turns back to higher

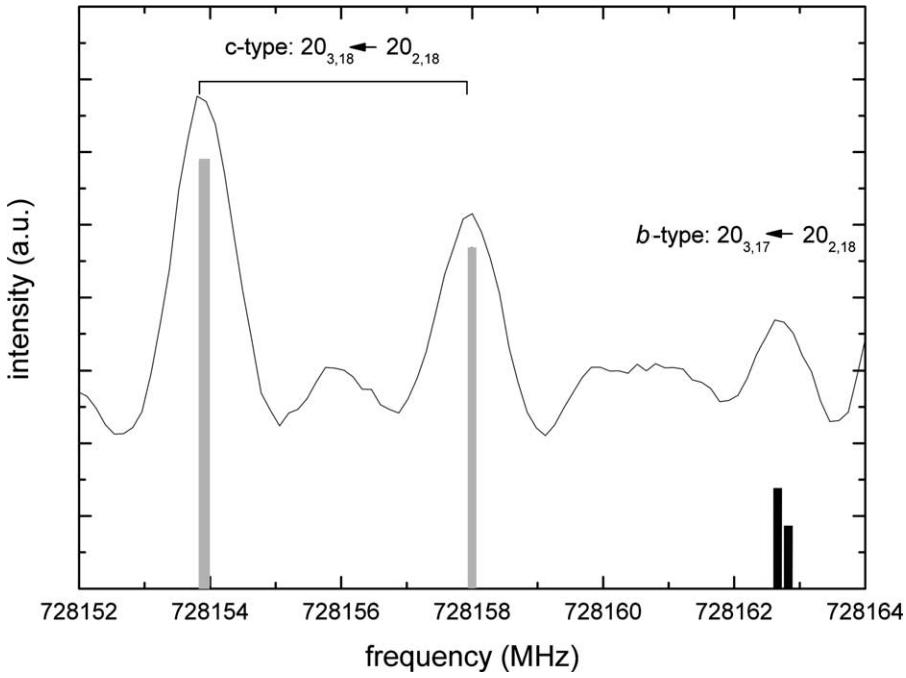

Fig. 1. Torsional splitting of the $J=20$ c-type (grey) and b-type (black) transitions in the ${}^{r}Q_2$ branch.

frequencies at higher J values. This behavior can also be seen from Fig. 3, where the transitions with $J=29$, 30, 31 follow increasing frequencies.

From the analysis of the Q-branch transitions, we obtained molecular spectroscopic parameters which allowed for the prediction of accurate P- and R-branch transition frequencies. We found 12 transitions within the spectral range of our measurements which belong to transitions of the ${}^{r}R_0$- and ${}^{r}R_1$-branch. While Q-branch transitions allow only for determination of the molecular constants $A-(B+C)/2$, $(B-C)/4$, additional R- or P-branch transitions reveal the constants A, B, and C, separately. We used Pickett's program *spfit/spcat* [26] employing a standard Watson type Hamiltonian in S reduction to fit the data. Due to the high accuracy of the measurements all quartic centrifugal distortion constants D and the sextic constants H_{JK} and H_K as well as h_2 and h_3 were determined. A weak Coriolis interaction of closely related states was found and has been considered by the G coriolis interaction term. The two components due to tunnel splitting were treated as two separate states and the ΔE gives the energy separation of the two states for $K_a=0$. The weighted root mean-squares deviation of all fitted lines is found to be 0.996, which indicates that all measured transitions can be reproduced to their experimental uncertainties. All constants of the fit are given in Table 1. Instead of giving the parameters for the upper and lower torsional state, the average constant and half of the difference between the upper and the lower sub-state is given.

The line splitting due to the tunnel effect has been measured to be about 4.5 MHz for all c-type transitions of the ${}^{r}Q_2$ band and less than 300 kHz for b-types which corresponds to the resolution of the spectrometer. Both b- and c-type transitions obey the selection rule $\Delta K_a=\pm 1$ and thus carrying information on the tunnel splitting δ'_{K_a} and δ''_{K_a} of upper K'_a and lower K''_a state levels. For c-type transitions the two components of line doublets are separated by $\delta_{K'_a}+\delta_{K''_a}$, whereas the corresponding line splitting of b-type transitions is calculated from $|\delta_{K'_a}-\delta_{K''_a}|$ (see e.g. [25]). The line splitting $\Delta\nu_{1,0}=\delta_1+\delta_0$ for all ${}^{r}R_0$ c-type transitions was found to be 3.4 MHz, the splitting of ${}^{r}R_1$ c-types is $\Delta\nu_{2,1}=\delta_2+\delta_1=$ 2.2 MHz and for the ${}^{r}Q_2$ doublets we found $\Delta\nu_{3,2}=\delta_3+\delta_2=4.5$ MHz. On the other hand, all measured doublets of b-type ${}^{r}R_{0,1}$ and ${}^{r}Q_2$ transitions are not resolved and

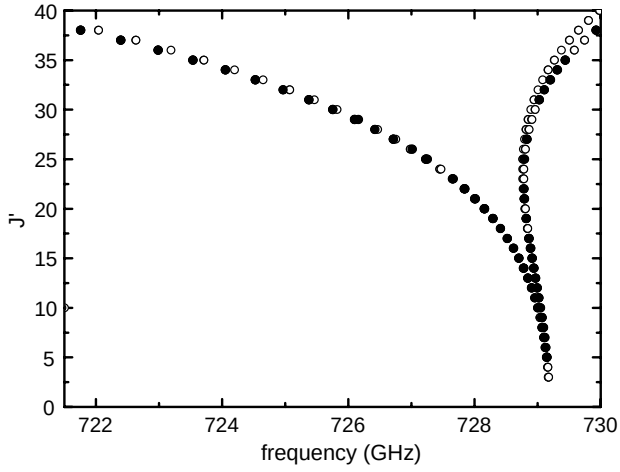

Fig. 2. Fortrat diagram of the HSOD ${}^{r}Q_2$ branch at 729 GHz. With increasing J rotational quantum numbers the lines split into a series of additional components, which are caused by two effects: (i) the inertial asymmetry splitting (larger splitting) and (ii) the separation into b- and c-type transitions (smaller splitting). The full circles represent measured transitions while empty circles are calculated from a least square fit of all data.

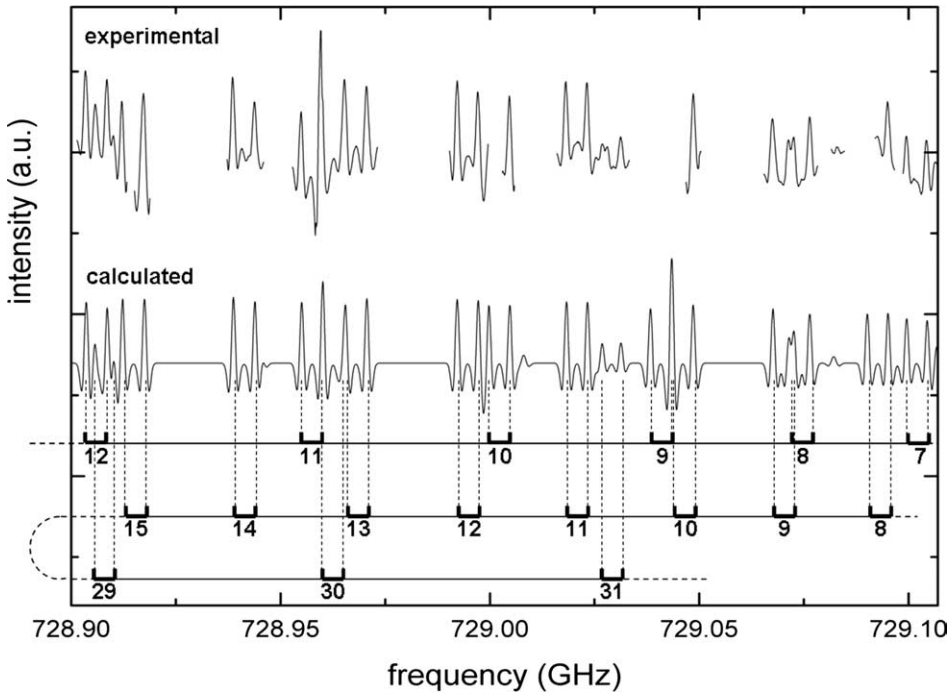

Fig. 3. Band-head of the $^{r}Q_2$ branch of HSOD. At the top experimental data are shown. A calculated spectrum and the assignment of the *c*-type transitions for both asymmetry components ($J_{3,J-2} \leftarrow J_{2,J-2}$ in the upper trace, $J_{3,J-3} \leftarrow J_{2,J-1}$ in the lower trace) are mapped below the experimental data. The *K*-independent torsional splitting for each transition is clearly to be seen.

thus the terms $\Delta\nu_b = |\delta_{K'_a} - \delta_{K''_a}|$ are small in all cases, indicating that the δ_{K_a} have to be almost equivalent for all K_a and in the order of 2 MHz, which is in good agreement to the K_a independent value of 3.4 MHz obtained by Quack *et al*. [10] from *ab initio* calculations.

The ratio of measured line intensities of transitions belonging to *c*- and *b*-type transitions have been used to derive the ratio of the dipole components μ_c/μ_b. For the intensities of *b*-type transitions we took into account that the torsional splitting is not resolved and thus *b*-type transitions gain in intensities by overlapping of lines. We obtained a ratio $\mu_c/\mu_b = 2.4(3)$ from the measurements, which is in good agreement with the theoretically predicted value of 1.9 ($\mu_c = 1.4908$ D, $\mu_b = 0.7854$ D).

5. Structure of oxadisulfane

Anharmonicities of the molecular potential cause the rotational constants to change with vibrational excitation. Applying perturbation theory to the vibration-rotation Hamiltonian leads to an expansion of the rotational constants B_v of the *v*th vibrational state *r* in powers of $v + 1/2$ which are linear to second-order perturbation. The dependence of the rotational constants on the vibrational quantum numbers *v* are conventionally denoted by α_r^B, where the subscript refers to the *r* normal coordinate. In this approximation, the molecular rotational constant for the vibrational ground state B_0 is related to the equilibrium rotational constant B_e by

Table 1
Ground state molecular parameters (MHz) of HSOD

Parameter	Theoretical value[a]	Scaled theoretical value[b]	Experimental value
A	159,973.5	159,903.7	159,965.19(45)
$\Delta A/2$			2.375(248)
B	14,133.1	14,134.9	14,132.202(40)
$\Delta B/2$			0.00259(82)
C	14,023.5	14,021.9	14,020.683(41)
$\Delta C/2$			−0.00314(85)
$D_J \times 10^3$	19.7471	20.7196	20.729(52)
$\Delta D_J/2 \times 10^3$			−0.183(84)
$D_{JK} \times 10^3$	277.779	292.706	290.639(45)
D_K	3.57255	4.02488	3.289(86)
$\Delta D_K/2$			0.786(74)
$d_1 \times 10^3$	−0.13776	−0.15047	−0.1530(42)
$\Delta d_1/2 \times 10^3$			−0.00219(68)
$d_2 \times 10^3$	0.39006	0.51376	0.509411(93)
$\Delta d_2/2 \times 10^3$			0.000161(85)
$H_{JK} \times 10^6$			−2.378(68)
H_K			−0.1178(109)
$h_2 \times 10^9$			−6.66(43)
$h_3 \times 10^9$			3.945(235)
ΔE	3.45[c]		3.36(36)
G_a			0.3567(147)
wrms[d]			0.996
μ_c/μ_b[d]	1.9		2.4(3)

[a] *A*, *B*, *C*: CCSD(T)/cc-pCVQZ + CCSD(T)/cc-pVTZ vibrational corrections; centrifugal distortion parameters: CCSD(T)/cc-pVTZ; dipole moment: MP2/cc-pVTZ.
[b] See text.
[c] Calculated by Quack and Willeke [10] (RPH with MP2/aug-cc-pVTZ basis set).
[d] Dimensionless.

Table 2
Empirical geometrical parameters (distances in angstrom, angles in degrees) for oxadisulfane

Geometrical parameter	CCSD(T)/cc-pCVQZ [3]	Empirical r_e^{emp}
R(SO)	1.6619	1.6616(1)
R(SH)	1.3414	1.3420(2)
R(OH)	0.9601	0.9606(3)
α(OSH)	98.55	98.57(5)
α(SOH)	107.01	107.19(3)
τ(HSOH)	91.29	90.41(11)

$$B_e = B_0 + \frac{1}{2}\sum_r \alpha_r^B. \quad (1)$$

For an N atoms counting nonlinear molecule the summation has to be taken over the $r=3N-6$ vibrational modes. The rotational constant B_e is related to the principal moment of inertia I_b by $B_e=h/(8\pi^2 cI_b)$ and can thus be used to determine the molecular structure. Within the Born–Oppenheimer approximation, the r_e equilibrium geometry is the same for all isotopomers and can be derived from a least-squares fit of molecular bond distances and angles to a set of rotational constants or moments of inertia. The vibration–rotation correction terms α_r^B can be derived experimentally from the rotation constants B_{v_r} for a vibrationally excited state with quantum number v_r for the r-*th* mode by

$$\alpha_r^B = (B_0 - B_{v_r})/v_r. \quad (2)$$

When rotational constants of vibrational states are not available from experiments, calculated α_r^B values can be used instead to derive an *empirical* equilibrium structure r_e^{emp}.

An accurate theoretical structure of HSOH has been obtained from CCSD(T)/cc-pCVQZ *ab initio* calculations [3]. All structural parameters are given in Table 2. To derive an empirical equilibrium structure of HSOH the rotational constants A_0, B_0, and C_0 of HSOD together with previously published rotational constants of HSOH, $H^{34}SOH$, and DSOD [3,9] have been used. Empirical equilibrium constants A_e^{emp}, B_e^{emp} and C_e^{emp} according to Eq. (1) have been derived for these isotopomers using vibration–rotation correction terms obtained from CCSD(T)/cc-pVTZ calculations of the harmonic and anharmonic force fields (see Table 3). The three bond lengths R(OH), R(SH) and R(SO) as well as the bond angles α(OSH), α(SOH), and the dihedral angle τ(HSOH) were fitted to the empirical equilibrium constants of the four isotopomers using a least-squares fit analysis (see, for example, Ref. [27]). All results of the fit are given in Table 2 and the structure of HSOH is depicted in Fig. 4. The geometrical parameters derived from the empirical approach are in excellent agreement with pure *ab initio* values based on CCSD(T)/cc-pCVQZ calculations, with the largest deviation seen in the torsional angle.

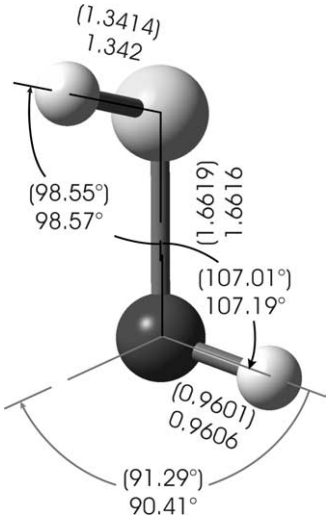

Fig. 4. Empirical geometrical equilibrium structure of HSOH. Theoretical results as obtained at the CCSD(T)/cc-pCVQZ level are given in parentheses. Bond lengths are given in angstrom, angles in degrees.

Table 3
Rotational constants and vibrational corrections (MHz) for HSOH and its isotopomers

Parameter	Experimental value, $v=0$	$\frac{1}{2}\sum_r \alpha_r$ [a] (CCSD(T)/cc-pVTZ)
HSOH [3]		
A	202,069.05431(134)	1431.9
B	15,281.956620(123)	118.7
C	14,840.216440(121)	136.3
$H^{34}SOH$ [3]		
A	201,739.7641(129)	1431.1
B	15,001.43940(38)	116.0
C	14,573.77816(39)	133.1
DSOD [11]		
A	106,850.4937(55)	513.9
B	13,865.38319(173)	89.1
C	13,173.54491(227)	106.8
HSOD (this work)		
A	159,965.20(44)	946.2
B	14,132.204(40)	107.5
C	14,020.685(41)	111.6

[a] α_r are the vibration rotation interaction constants for all normal modes r.

6. Conclusion

Precise spectroscopic data of HSOD have been obtained and compared to high level CCSD(T) calculations. The experimentally derived molecular constants are in excellent agreement with the theoretically predicted values (see Table 1). Furthermore, the data on HSOD have been used together with previously published experimental results on HSOH, $H^{34}SOH$, and DSOD to derive for the first time structural parameters of oxadisulfane in an empirical approach. The agreement between experimentally and theoretically obtained values is excellent and emphasizes the high quality of *ab initio* calculations. On the other hand it shows the superb quality of high resolution data obtained with the Cologne terahertz spectrometer. The structure of HSOH is now well understood and predictions for all other isotopomers, such as DSOH, $HS^{18}OH$, are now feasible. DSOH is expected to be

more asymmetric ($\kappa = -0.9806$) than all other isotopomers studied so far and experimental results will be published in a forthcoming paper. Furthermore vibrational excited states of HSOH and its isotopomers will yield experimental values on the vibration–rotation correction terms α_r.

Acknowledgements

This work has been supported by the Deutsche Forschungsgemeinschaft via research grant SFB 494. In addition, JG acknowledges support from the Deutsche Forschungsgemeinschaft and the Fonds der Chemischen Industrie.

References

[1] J.M. Flaud, C. Camy-Peyret, J.W.C. Johns, B. Carli, J. Chem. Phys. 91 (1989) 1504–1510.
[2] S. Urban, E. Herbst, P. Mittler, G. Winnewisser, K.M.T. Yamada, J. Mol. Spectrosc. 137 (1989) 327–353.
[3] G. Winnewisser, F. Lewen, S. Thorwirth, M. Behnke, J. Hahn, J. Gauss, E. Herbst, Chem. Eur J. 9 (2003) 5501–5510.
[4] G. Winnewisser, M. Winnewisser, W. Gordy, J. Chem. Phys. 49 (1968) 3465–3478.
[5] P. Helminger, W.C. Bowmann, F.C. De Lucia, J. Mol. Spectrosc. 85 (1981) 120–130.
[6] R.R. Smardzewski, M.C. Lin, J. Chem. Phys. 66 (1977) 3197–3204.
[7] M. Iraqi, H. Schwarz, Chem. Phys. Lett. 221 (1994) 359–362.
[8] M. Behnke, PhD Thesis, Universität zu Köln, Shaker, Aachen, 2001.
[9] M. Behnke, J. Suhr, S. Thorwirth, F. Lewen, H. Lichau, J. Hahn, J. Gauss, K.M.T. Yamada, G. Winnewisser, J. Mol. Spectrosc. 221 (2003) 121–126.
[10] M. Quack, M. Willeke, Helv. Chim. Acta 86 (2003) 1641–1652.
[11] S. Brünken, M. Behnke, S. Thorwirth, K.M.T. Yamada, T. Giesen, F. Lewen, J. Hahn, G. Winnewisser, J. Mol. Struct. 742 (2005) 237–242.
[12] H. Wallmeier, W. Kutzelnigg, J. Am. Chem. Soc. 101 (1979) 2084.
[13] T.J. Lee, N.C. Handy, J.E. Rice, A.C. Scheiner, H.F. Schaefer III, J. Chem. Phys. 85 (1986) 3930–3938.
[14] J.A. Altmann, N.C. Handy, V.E. Ingamells, Int. J. Quantum Chem. 57 (1996) 533–542.
[15] J.A. Altmann, N.C. Handy, V.E. Ingamells, Mol. Phys. 92 (1997) 339–352.
[16] J.A. Altmann, N.C. Handy, Phys. Chem. Chem. Phys. 1 (1999) 5529–5536.
[17] G. Menconi, D.J. Tozer, Phys. Chem. Chem. Phys. 5 (2003) 2938–2941.
[18] H. Beckers, S. Esser, T. Metzroth, M. Behnke, H. Willner, J. Gauss, J. Hahn, Chem. Eur. J. 12 (2006) 832–844.
[19] G. Winnewisser, Vib. Spectrosc. 8 (1995) 241.
[20] K. Raghavachari, G.W. Trucks, J.A. Pople, M. Head-Gordon, Chem. Phys. Lett. 157 (1989) 479–483.
[21] K.A. Peterson, T.H. Dunning, J. Chem. Phys. 118 (2002) 10548–10560.
[22] I.M. Mills, in: K.N. Rao, C.W. Matthews (Eds.), Modern Spectroscopy: Modern Research, Academic Press, New York, 1972, p. 155.
[23] T.H. Dunning, J. Chem. Phys. 90 (1989) 1007–1023.
[24] J. Gauss, J.F. Stanton, Chem. Phys. Lett. 276 (1997) 70–77.
[25] K.M.T. Yamada, G. Winnewisser, P. Jensen, J. Mol. Struct. 695–696 (2004) 323–337.
[26] H.M. Pickett, J. Mol. Spectrosc. 148 (1991) 371–377.
[27] F. Pawlowski, P. Jørgensen, J. Olsen, F. Hegelund, T. Helgaker, J. Gauss, K.L. Bak, J.F. Stanton, J. Chem. Phys. 116 (2002) 6482–6496.